

Variable factor S-transform seismic data analysis

Todor I. Todorov and Gary F. Margrave

ABSTRACT

Most of today's geophysical data processing and analysis methods are based on the assumption that the seismic signal is stationary and employ an extensive use of Fourier analysis. However due to various attenuation mechanisms of the Earth, the seismic signal is not stationary. The short-time Fourier transform (Gabor transform) has been developed to deal with nonstationary signals. The variable factor S-transform is an extension of the Gabor transform and provides better time-frequency decomposition of a nonstationary signal for all frequencies. An S-transform deconvolution method is developed as an extension of the nonstationary Gabor deconvolution reported in the literature. The new method is tested on a constant Q synthetic data and shows superior results over the traditional stationary Wiener deconvolution and an improvement over the nonstationary Gabor deconvolution. In a separate application an f-t-x CDP noise attenuation method is developed. A synthetic example proves the effectiveness of the f-t-x noise attenuation for both, high-amplitude linear noise and random noise.

INTRODUCTION

Most of today's geophysical data processing and analysis are based on the assumption that the seismic signal is stationary and employ an extensive use of Fourier analysis. However due to various attenuation mechanisms of the Earth, the seismic signal is not stationary. Margrave (1998) has presented the theory of the nonstationary linear filtering, which is a better approximation to the physical phenomena of seismic wave propagation in the earth over the traditional stationary convolutional model. Margrave and Lamoureux (2001) presented a nonstationary deconvolution based on the Gabor transform, known as short-time Fourier Transform as well (Mertins, 1999). Since the introduction of the Gabor transform (Gabor, 1946) various time-frequency decomposition methods has been proposed to improve on the time-frequency resolution and other properties of the transform (Mertins, 1999). One such transform is the S-transform (Stockwell, 1996). This work is concerned with the investigation of the S-transform application for nonstationary seismic deconvolution and noise attenuation.

THE VARIABLE FACTOR S-TRANSFORM

The Fourier transform

The Fourier transform is a fundamental tool in seismic data processing and analysis. It applies to almost all stages of processing. A number of seismic attributes used in interpretation are also based on the Fourier transform. It completely describes a seismic trace as a sum of complex sinusoids – each with unique amplitude, frequency, and phase.

The analysis of a signal $h(t)$ is achieved by the forward Fourier transform

$$H(f) = \int_{-\infty}^{+\infty} h(t)e^{-i2\pi ft} dt, \quad (1)$$

and its synthesis by the inverse Fourier transform

$$h(t) = \int_{-\infty}^{+\infty} H(f)e^{i2\pi ft} df, \quad (2)$$

where t is the time variable, f is frequency, and $H(f)$ is called the Fourier spectrum. It is a complex function and can be expressed in terms of its real $H_R(f)$ and imaginary $H_I(f)$ components

$$H(f) = H_R(f) + iH_I(f). \quad (3)$$

The Fourier spectrum can be written as a function of the amplitude spectrum $A(f)$ and the phase spectrum $\Phi(f)$

$$H(f) = A(f)e^{i\Phi(f)} \quad (4)$$

which are computed from the following equations

$$A(f) = \sqrt{H_R^2(f) + H_I^2(f)} \quad (5)$$

$$\Phi(f) = \tan^{-1} \frac{H_I(f)}{H_R(f)} \quad (6)$$

One drawback of the Fourier transform is that it only produces the time-average spectrum. Figure 1 is a display of a particular signal and its amplitude and phase spectra. By examining them one can conclude the frequency content of the signal, i.e. the signal contains 10, 20, 50, 100, and 150 Hz frequency components. Figure 2 shows how this signal was constructed.

The Fourier transform correctly tells us which frequencies exist in the signal, however they are not present all the time. So the Fourier transform gives the frequency information of the signal, but does not tell us when in time these frequency components exist. In other words, Fourier transform is appropriate tool for frequency analysis of stationary signals, i.e. signals whose frequency content does not change in time. For nonstationary signals, whose frequency content changes in time, we need both the time and the frequency dependence simultaneously.

The short-time Fourier transform

To overcome the limitations of the Fourier transform in analysing nonstationary signals, Gabor (1946) introduced the short-time Fourier transform, known as Gabor transform as well. The concept is simple: multiply the signal $h(t)$ with an analysis window and then compute the Fourier transform of the windowed signal. This gives us the local Fourier spectrum of the signal. By shifting the analysis window along the signal, we get a time-frequency spectrum of the signal.

Mathematically, the Gabor transform is defined as (e.g. Mertins, 1999)

$$G(\tau, f) = \int_{-\infty}^{+\infty} h(t)w(t - \tau)e^{-i2\pi ft} dt \quad (7)$$

where $w(t)$ is the analysis window and $G(\tau, f)$ is the complex Gabor spectrum. In his work Gabor has chosen a Gaussian window

$$w(t) = \frac{1}{\sqrt{2\pi}\sigma} e^{-t^2/2\sigma^2} \quad (8)$$

where σ is the standard deviation. By applying the Gabor transform to a signal, we decompose one dimensional function $h(t)$ into a two dimensional one $G(\tau, f)$. This process is known as time-frequency analysis. The goal is to tell not only which frequencies exist, but when they appear as well. We try to achieve the best possible time and frequency resolution as well. However, choosing a short time window leads to good time resolution, but low frequency resolution. On the other hand, a long time window yields low time resolution, but good frequency resolution.

The maximum possible resolution is governed by the uncertainty principle (e.g. Mertins, 1999)

$$\Delta t \Delta \omega \geq \frac{1}{2} \quad (9)$$

where $\Delta t \Delta \omega$ is the area in the time frequency plane covered by a particular window. The equity sign, i.e. the best time-frequency resolution, is achieved only if $w(t)$ is a Gaussian function (e.g. Mertins, 1999).

The Gabor transform synthesis is achieved by integration over frequency and over window position

$$h(t) = \int_{-\infty}^{+\infty} \int_{-\infty}^{+\infty} G(\tau, f) \gamma(t - \tau) e^{i2\pi ft} d\tau df \quad (10)$$

where the synthesis window $\gamma(t)$ must satisfy the condition

$$\int_{-\infty}^{+\infty} w(t) \gamma(t) dt = 1 \quad (11)$$

Figure 3 is a display of the Gabor time-frequency decomposition of the composed signal with a variable with windows. The CREWES Project MATLAB toolbox function *fgabor* was used. The window step was chosen to be equal to the sampling rate of the signal, 0.002 sec. The maximum redundancy is chosen for a fair comparison with the later discussed S-transform. Figure 3 a) is the Gabor spectrum with 0.01 seconds width, which obviously is a poor choice and leads to smearing along the frequency axis. Note the very high time resolution. Figure 3 b) is the Gabor spectrum with 0.05 seconds width. The frequency resolution is much better, except for the 10 and 20 Hz components. By

increasing the window width to 0.1 seconds (Figure 3 c)) we achieve a very good frequency resolution, however we have lost the good time resolution for the 150 Hz component. By increasing the window width to 0.2 we loose completely the time resolution of the high-frequency component. By examining the plots, one can conclude that a window with of 0.05 sec gives a good time-frequency representation of the 150 Hz component, however the window with 0.1 width give us the good time-frequency representation of the lower frequency components of 10 and 20 Hz. So with the Gabor transform, for a particular window choice, we can achieve good time-frequency representation for a particular frequency range, but poor time or frequency resolution outside of the band.

The S-transform and the variable factor S-transform

To overcome the limitations of the short-time Fourier transform a variety of time-frequency decompositions have been proposed, notably the continuous wavelet transform (e.g. Mertins, 1999). This paper is particularly concerned with the S-Transform (Stockwell, 1996). It uniquely combines a frequency dependent resolution with simultaneously localizing the real and imaginary spectra. It is particularly appealing to geophysical signal analysis since it generates time-frequency decomposition versus time-scale decomposition in the continuous wavelet transform case. Frequency is preferred since it has a specific physical meaning.

The continuous S-transform of a signal $h(t)$ is defined by (Stockwell, 1996)

$$S(\tau, f) = \int_{-\infty}^{+\infty} h(t) \frac{|f|}{\sqrt{2\pi}} e^{-\frac{(\tau-t)^2 f^2}{2}} e^{-i2\pi ft} dt \quad (12)$$

where t and τ are time variables and f is frequency variable. The S-transform can be derived from the Gabor transform by defining the standard deviation σ of the Gaussian window to be a function of the frequency f

$$\sigma(f) = \frac{1}{|f|} \quad (13)$$

Since $S(\tau, f)$ is complex, we can define its amplitude $A(\tau, f)$ and phase $\Phi(\tau, f)$ spectrum in a similar way to the Fourier transform. The time average of the $S(\tau, f)$ gives the Fourier spectrum of $h(t)$ (Stackwell, 1996).

The inverse S-transform is given by (Stockwell, 1996)

$$h(t) = \int_{-\infty}^{+\infty} \left[\int_{-\infty}^{+\infty} S(\tau, f) d\tau \right] e^{i2\pi ft} df \quad (14)$$

The lossless invertibility of the S-transform allows for filtering in the time-frequency domain.

The original S-transform proposed by Stockwell set the standard deviation of the Gaussian window proportional to the inverse of the frequency (eq. 13). Manshinha et al (1997) introduced a constant factor k in the standard deviation of the analysis window

$$\sigma(f) = \frac{k}{|f|} \quad (15)$$

By increasing the factor k they have achieved better frequency resolution, with a corresponding loss of resolution in time. In their work they have suggested $k=3$.

Figure 4 a), b), c) is the S-transform amplitude spectrum of the signal from Figure 1 with factors 1, 2, and 3 respectively. We can notice good frequency-time resolution of the lower frequency components with factor 1, however poor frequency resolution for the mid and higher frequency components. Factor 2 improves the frequency resolution, however we start to lose the time resolution for the 10 Hz component. The mid-frequency range has good time-frequency resolution. With factor 3 we achieve a very good frequency resolution, however the time resolution of the low-frequency components is completely lost.

By examining the plots one can conclude that factor 1 is a good choice to achieve both time and frequency for low-frequency components, factor 2 for the mid-range components, and 3 for the higher frequencies. However in the Stockwell S-transform the factor is a constant number. We propose a Variable Factor S-transform, in which the factor is a function of the frequency as well

$$\sigma(f) = \frac{k(f)}{|f|} \quad (16)$$

$$S(\tau, f) = \int_{-\infty}^{+\infty} h(t) \frac{|f|}{\sqrt{2\pi k(f)}} e^{-\frac{(\tau-t)^2 f^2}{2k^2(f)}} e^{-i2\pi ft} dt. \quad (17)$$

The simplest way to define a variable k is by using a linear model. I define minimum factor at zero frequency, maximum factor at Nyquist frequency and linearly interpolate for any frequency in between. Figure 4 d) is the amplitude spectrum of the same signal using linear factor from 1 at zero frequency and 6 at Nyquist. We can see a good time-frequency resolution for all the present frequency components. The inverse transform can still be defined by equation (14).

S-TRANSFORM DECONVOLUTION

The convolutional model

The goal of the seismic deconvolution process is to compress the basic wavelet, remove multiples, and yield a representation of the subsurface reflectivity $r(t)$ (Yilmaz, 2001). The theoretical base of the majority of today's deconvolutional methods is the convolutional model, defined as

$$s(t) = w(t) * e(t) + n(t) \quad (18)$$

where

$s(t)$ is the recorded seismic trace,

$w(t)$ is the seismic wavelet,

$e(t)$ is the earth impulse response,

$n(t)$ is additive noise.

This simple equation may be interpreted in different ways (Margrave, 2005). In forward modeling, for example, one may choose to convolve a zero-phase wavelet with reflectivity derived from a sonic and density logs. The result is zero-offset, primaries only seismic trace, i.e. the impulse response in the above equation is the reflectivity. However, for a recorded seismic trace the impulse response is a superposition of various phenomena in addition to reflections only, like multiples, transmission losses, mode conversions, and so on. In general, the source wavelet is unknown and we end up with two unknowns to solve for: $w(t)$ and $r(t)$. In addition, the seismic wavelet can be regarded as the source wavelet or as a more complicated function combining the source wavelet with the near surface effects. To summarize, seismic wave propagation is a very complex phenomenon, and any deconvolution method is based on some simplifications and assumptions.

Wiener Deconvolution

Stationary Wiener deconvolution is one of the main processes applied in today's seismic data processing. It is based on the assumption that the seismic trace can be described as a convolutional process of the earth reflectivity $r(t)$ and a wavelet $w(t)$

$$s(t) = w(t) * r(t) + n(t) \quad (19)$$

The wavelet is described as 'the embedded wavelet', i.e. a wavelet that fits to the convolutional model. Since the prime goal of the deconvolution process is the recovery of the reflectivity, the actual components of the wavelet are not described and treated as a 'package'. Our goal is to derive an inverse filter $x(t)$ of the wavelet to derive the reflectivity. A number of further assumptions are made to accomplish this, the most important listed as follows (Yilmaz, 2001; Margrave, 2005):

- the wavelet does not change as it travels, i.e. we deal with a stationary process
- the wavelet is causal, minimum-phase
- the reflectivity is random, white sequence, i.e. the autocorrelation of the seismic trace is a scaled version of the autocorrelation of the wavelet
- the noise is white and stationary

The process of finding an m-length causal, inverse filter, based on the above assumptions, reduces to solving a linear system of equations

$$\begin{bmatrix} \phi_0 & \phi_1 & \phi_2 & \cdots & \phi_m \\ \phi_1 & \phi_0 & \phi_1 & \cdots & \phi_{m-1} \\ \phi_2 & \phi_1 & \phi_0 & \cdots & \phi_{m-2} \\ \vdots & \vdots & \vdots & \ddots & \vdots \\ \phi_m & \phi_{m-1} & \phi_{m-2} & \cdots & \phi_0 \end{bmatrix} \begin{bmatrix} x_0 \\ x_1 \\ x_2 \\ \vdots \\ x_m \end{bmatrix} = \begin{bmatrix} 1 \\ 0 \\ 0 \\ \vdots \\ 0 \end{bmatrix} \quad (20)$$

where ϕ_i is the i-th lag of the seismic trace autocorrelation. The system is solved using the least-squares approach. In practice, a small value is added to the zero-lag diagonal to ensure stability.

Gabor Deconvolution

Due to the subsurface attenuation, the recorded seismic trace is nonstationary by nature. The Winner deconvolution however is based on the stationary convolutional model, so the current seismic processing requires additional amplitude corrections. One can apply a geometrical spreading correction, but an absorption correction usually is not applied. A common way to go around the problem is to apply AGC. However, AGC smears the true relative amplitudes and the interpreters end up with incorrect amplitude maps and AVO analysis. So a nonstationary model is required.

The stationary convolutional model can be generalized to a nonstationary one (Margrave, 1998)

$$s(t) = \int_{-\infty}^{+\infty} w(t - \tau, \tau) r(\tau) d\tau \quad (21)$$

Based on the theory of the nonstationary filtering (Margrave, 1988) Margrave and Lamoureux (2001) define a nonstationary convolutional model based on the constant Q theory

$$S(f) = W(f) \int_{-\infty}^{+\infty} \alpha(f, t) r(t) e^{-i2\pi ft} dt \quad (22)$$

where capital letters denote the forward Fourier transform and

$$\alpha(t, f) = \exp\left(-\frac{\pi t}{Q(t)}(f + iH(f))\right) \quad (23)$$

The main advantage of the nonstationary formulation is the separation of the source wavelet and the attenuation process. The above nonstationary model may be expressed in Gabor domain

$$S_G(\tau, f) = W(f)\alpha(\tau, f)R_G(\tau, f) \quad (24)$$

where S_G and R_G are the Gabor transform of the seismic trace and the reflectivity. By invoking the some assumptions of the stationary deconvolution, like minimum-phase wavelet and white reflectivity, one can recover R_G , and by the inverse Gabor transform $r(t)$.

S-transform deconvolution

The Gabor deconvolution methodology is easily modified to perform a Variable Factor S-transform deconvolution. The only difference is that we substitute the Gabor transform with the S-transform. The following summarises the actual implementation

- compute the Variable Factor S-transform $S_S(\tau, f)$ of the input seismic trace
- apply hyperbolic smoothing to $S_S(\tau, f) \rightarrow S_S'(\tau, f)$ (Margrave and Lamoureux, 2001)
- estimate inverse operator $O_S(\tau, f)$ using minimum-phase assumption and $S_S'(\tau, f)$ multiply $S_S(\tau, f)$ with $O_S(\tau, f)$
- inverse S-transform

To compare the performance of the discussed deconvolution methods a synthetic trace example with a constant Q model is developed. Figure 5 is a display of a randomly generated reflectivity sequence and the corresponding synthetic trace with a minimum-phase wavelet and $Q=100$. Figures 6 and 7 are displays of the Gabor and the Variable Factor S-transform of the synthetic trace respectively. The clear decay of the spectrum in frequency and time shows the nonstationary nature of the signal. Figures 8, 9, and 10 display the results from performing the three types of deconvolution: Wiener, Gabor, and Variable Factor S-transform. The Wiener deconvolution fails to recover any of the high magnitude reflectivity. The Gabor deconvolution has recovered the reflectivity much better compared with the Wiener method, especially the high magnitude reflectivity. The Variable Factor shows an improvement over the Gabor method. Figures 11-16 are displays of the same experiment with $Q=60$. Similar conclusions can be made. Table 1 summarizes the results of the experiments.

Method	Total Abs. Error, Q=100	Total Abs. Error, Q=60
Wiener	7.2167	8.1997
Gabor	3.0356	3.0757
S-transform	2.6180	2.7349

Table 1: Absolute and relative errors for tested deconvolution methods.

F-T-X S-TRANSFORM NOISE ATTENUATION

The complex one-step-ahead prediction filter for random noise attenuation in f-x domain on stacked data was introduced by Canales (1984). Gulunay (1986) however states that the f-x method will not work on data with conflicting dips. Spitz (1991) developed the f-x trace interpolation. The above techniques transform the data from t-x to f-x domain using the Fourier transform. We have already argued that the seismic trace is nonstationary, so a time-frequency transform is better suited to describe it. The noise, especially source noise and low / high frequency bursts in data, is not stationary. This type of noise is present for a limited period of time. The ground roll is highly dispersive in nature, so different frequency components will reside in different locations on the f-t-x space. This makes the S-transform a very attractive tool to design a noise attenuation algorithm.

We propose a new method for noise attenuation on NMO-corrected CDP gather based on the S-transform. The method involves

- transform the CDP data from t-x domain to f - τ -x domain using the S-transform for each f, τ
- define the array $d(f=\text{const}, \tau=\text{const}, x)$
- for a data point $d(x_i)$ design a complex prediction filter in x-direction from the surrounding samples ..., $d(x_{i-1}), d(x_{i+1}), \dots$
- keep the error between the actual and the predicted value for each $d(x_i)$
- substitute the actual value with the predicted one for the sample $d(x_i)$ with the largest error
- next τ, f
- inverse S-transform

Note that only one sample for a particular τ, f is changed. This assures that the non-noisy samples are not altered and the noise does not creep out to the noise-free samples. The same process can be repeated as a second iteration on the filtered section if necessary.

The following example explains the filter design.

Problem: for a particular f, τ predict $d(x_i)$ using L surrounding samples by designing a prediction filter $g(x)$:

- form the following system of equations (in matrix form, $L=6$)

$$\begin{bmatrix} 0 & d(x_{i-2}) & d(x_{i-1}) & d(x_{i+1}) & d(x_{i+2}) & d(x_{i+3}) \\ d(x_{i-3}) & 0 & d(x_{i-1}) & d(x_{i+1}) & d(x_{i+2}) & d(x_{i+3}) \\ d(x_{i-3}) & d(x_{i-2}) & 0 & d(x_{i+1}) & d(x_{i+2}) & d(x_{i+3}) \\ d(x_{i-3}) & d(x_{i-2}) & d(x_{i-1}) & 0 & d(x_{i+2}) & d(x_{i+3}) \\ d(x_{i-3}) & d(x_{i-2}) & d(x_{i-1}) & d(x_{i+1}) & 0 & d(x_{i+3}) \\ d(x_{i-3}) & d(x_{i-2}) & d(x_{i-1}) & d(x_{i+1}) & d(x_{i+2}) & 0 \end{bmatrix} \begin{bmatrix} g(x_{i-3}) \\ g(x_{i-2}) \\ g(x_{i-1}) \\ g(x_{i+1}) \\ g(x_{i+2}) \\ g(x_{i+3}) \end{bmatrix} = \begin{bmatrix} d(x_{i-3}) \\ d(x_{i-2}) \\ d(x_{i-1}) \\ d(x_{i+1}) \\ d(x_{i+2}) \\ d(x_{i+3}) \end{bmatrix} \quad (25)$$

- solve for $g(x)$ using the truncated singular value decomposition (Aster et al, 2005)
- predict $d(x_i)$

A synthetic CDP model was generated to test the concept (Figure 17). Figure 18 shows the primaries only and Figure 19 the added noise, which contains a low-frequency, high amplitude linear event and a noisy trace. Figure 20 is the result of the f-t-x noise attenuation with a single iteration and Figure 21 is the removed noise. Most of the low-frequency high amplitude noise has been removed and the random noise has been removed as well even with a single iteration since they has different frequency content. Figure 22 is the filtered CDP gather after a second iteration and Figure 23 is the removed noise after both iterations. We can conclude that the noise has been removed successfully while the non-noisy amplitude has not been altered. The described method can be used as a trace interpolator in NMO-corrected CDP-gathers and shot-gathers as well.

CONCLUSIONS

The Variable Factor S-transform shows a better simultaneous time-frequency resolution than the Gabor transform and the traditional S-transform. The deconvolution method based on the Variable Factor S-transform is superior over the traditional Wiener deconvolution and improvement over the recently developed Gabor deconvolution. The f-t-x noise attenuation algorithm has shown a good potential and further testing is needed. However the S-transform is computationally expensive and further work needs to be done to investigate possible performance improvements.

FUTURE WORK

The Variable Factor S-transform have shown some encouraging result so far. We consider it a valuable tool for seismic data processing and analysis and we are planning some further work with it.

Some examples are:

- implement a frequency domain S-transform computation for better computational performance
- investigate the redundancy in the S-transform
- develop a surface-consistent S-transform deconvolution

- Q estimation
- test the f-t-x noise attenuation on a more complicated model with AVO and NMO-stretch, and on real data

REFERENCES

- Aster, R., Borchers, B., and Thurber, C., 2005, *Parameter Estimation and inverse problems*: Elsevier Academic Press.
- Canales, L., 1984, Random noise reduction: 54th Annual SEG Meeting, Expanded Abstracts, 525-527.
- Gabor, D., 1946, Theory of communication: *J. IEEE (London)*, 93, 429-457.
- Gulunay, N., 1986, F-X decon and complex Wiener prediction filter: 56th Annual SEG Meeting, Expanded Abstracts, 279-281.
- Margrave, G., 1998, Theory of nonstationary linear filtering in the Fourier domain with application to time-variant filtering: *Geophysics*, 63, 244-259.
- Margrave, G., and Lamoureux, M., 2001, Gabor deconvolution: The CREWES Project Research Report, 13, 241-276.
- Margrave, G., 2005, *Seismic Processing Fundamentals*: CSEG Course Notes.
- Mansinha, L., Stockwell, R., and Lowe, R., 1997, Local S-spectrum analysis of 1-D and 2-D data: *Physics of the Earth and Planetary Interiors*, 103, 329-336.
- Mertins, A., 1999, *Signal Analysis*: John Wiley and Sons.
- Spitz, S., 1991, Seismic trace interpolation in the f-x domain: *Geophysics*, 56, 785-794.
- Stockwell, R., Mansinha, L., and Lowe, R., 1996, Localization of the complex spectrum: The S-transform: *IEEE Trans. Signal Processing*, 44, 998-1001.
- Yilmaz, O., 2001, *Seismic data analysis*: SEG.

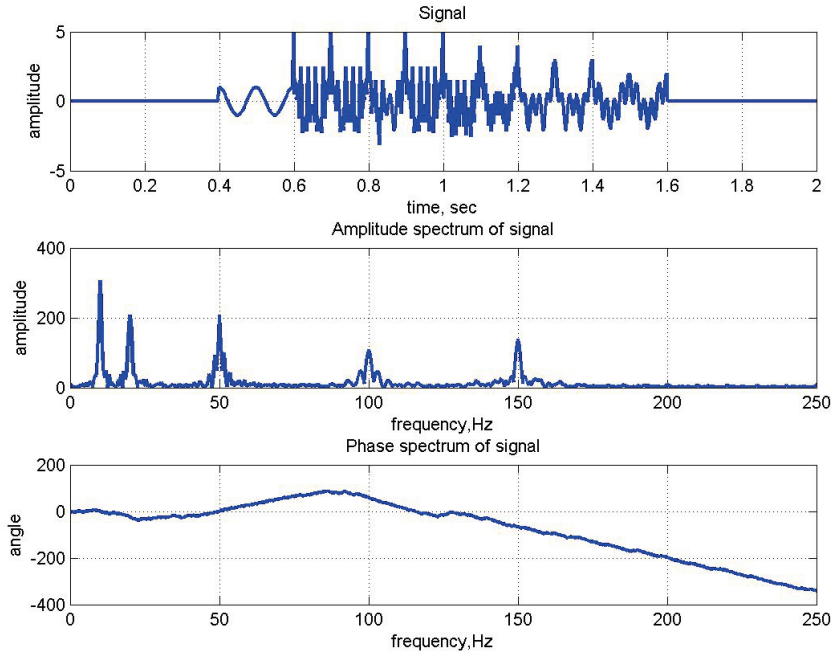


Figure 1: Fourier transform of a particular signal.

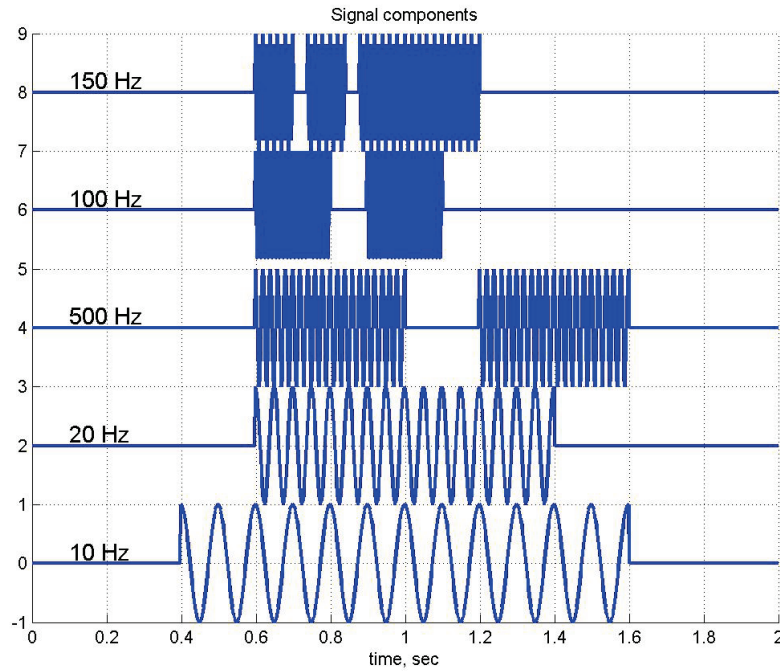


Figure 2: Complex sinusoids used to construct the signal.

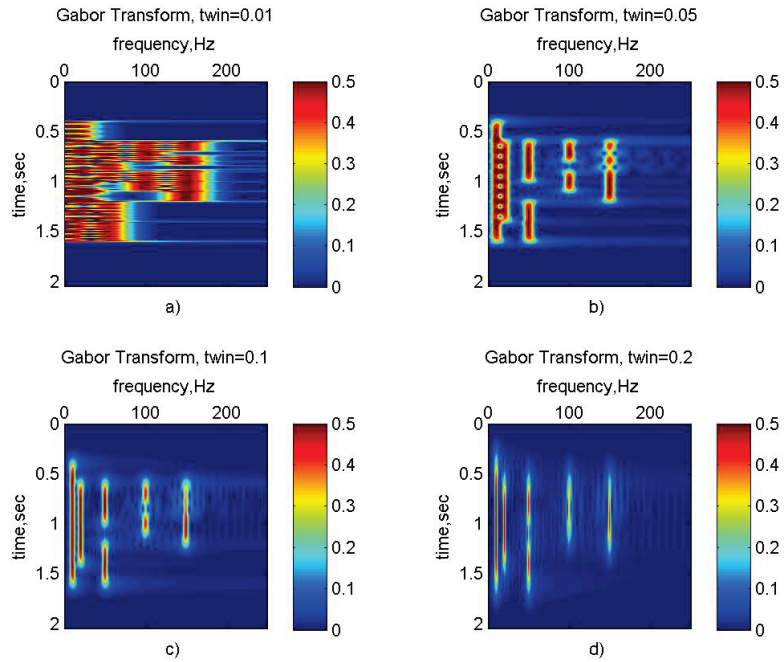


Figure 3: Gabor transform of the signal in Figure 1 with different windows: a) 0.01 sec., b) 0.05 sec., c) 0.1 sec., d) 0.2 sec.

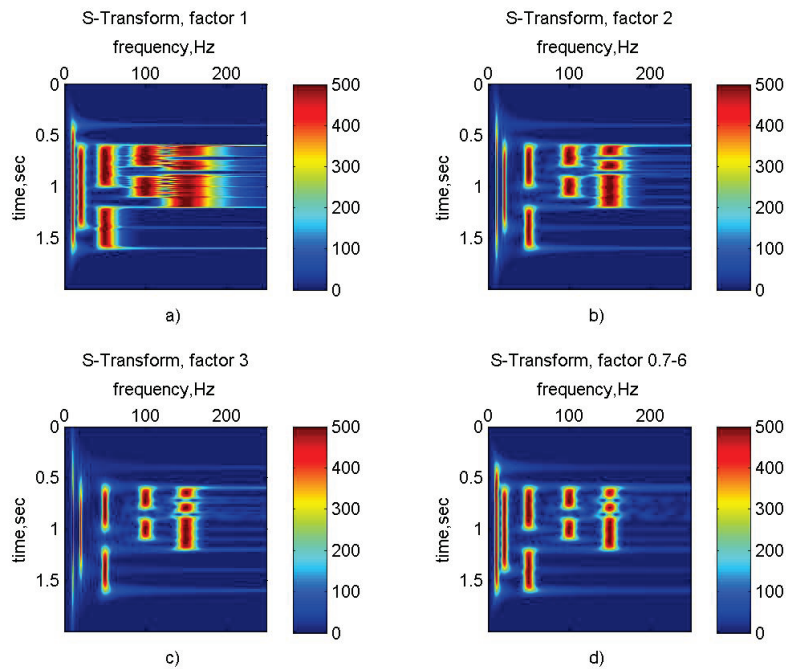


Figure 4: S-transform with factor: a) 1, b) 2, c) 3, d) 0.7-6

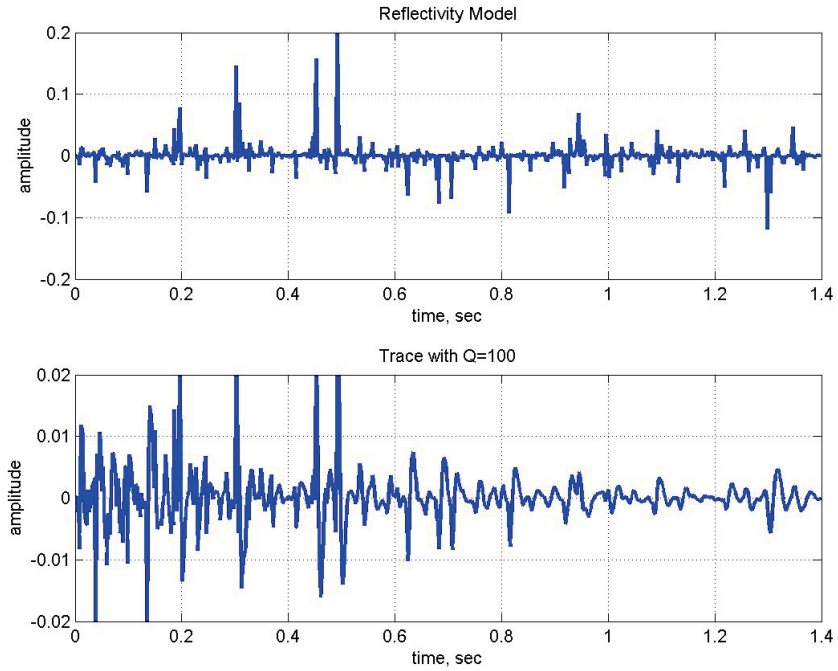


Figure 5: A random reflectivity model and a synthetic trace with a minimum-phase wavelet and $Q=100$.

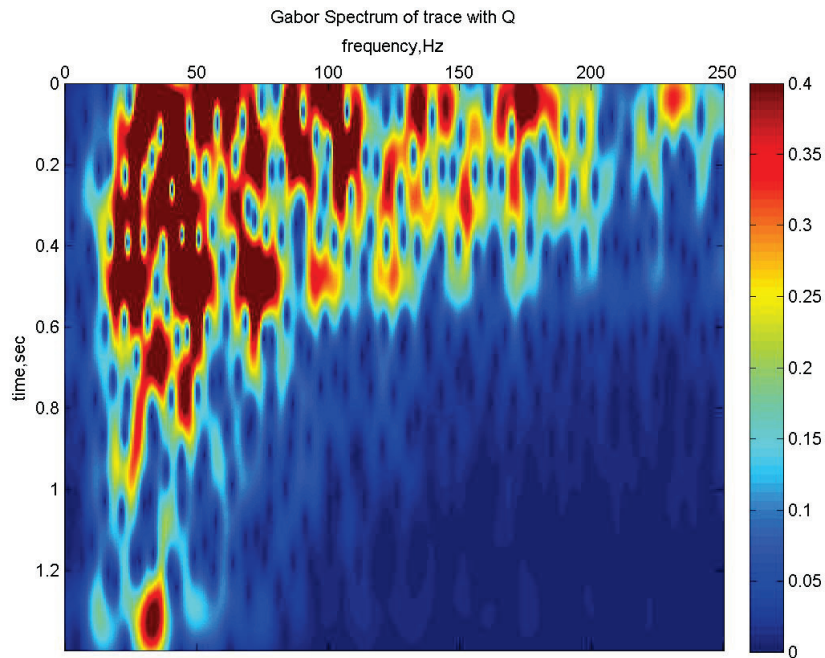


Figure 6: Gabor transform of the synthetic trace with $Q=100$.

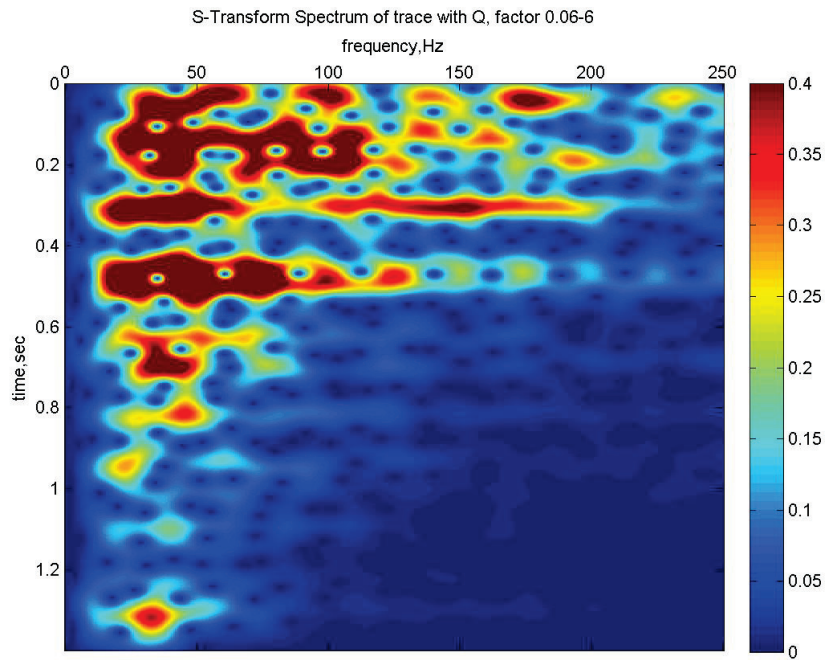


Figure 7: Variable factor S0transform of the synthetic trace with Q=100.

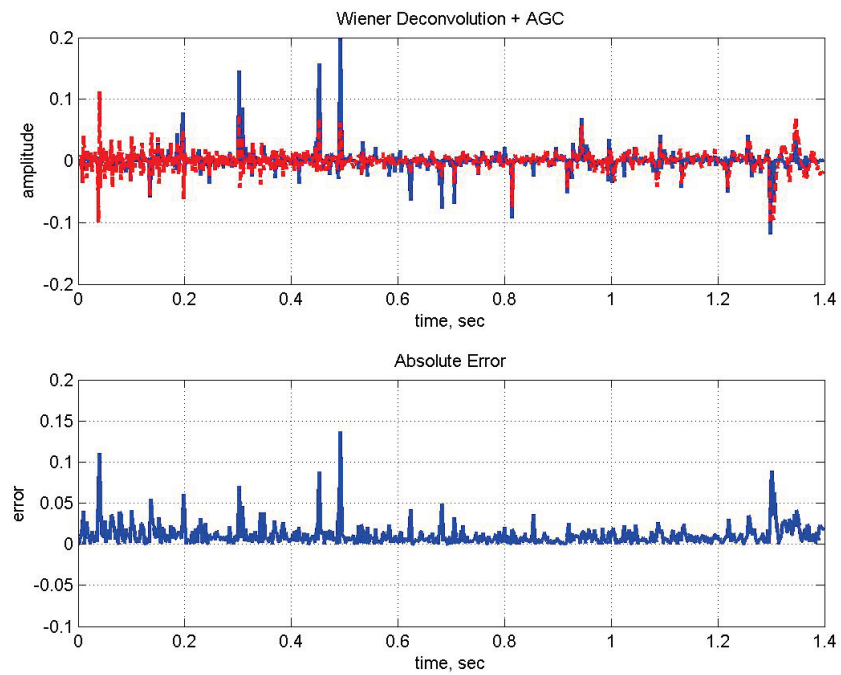


Figure 8: Wiener deconvolution of the synthetic trace with Q=100.

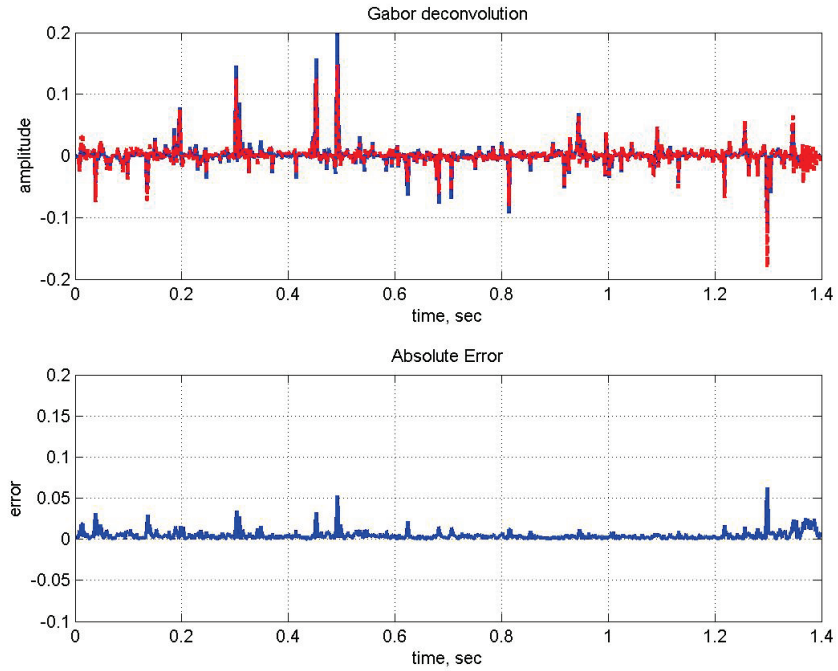


Figure 9: Gabor deconvolution of the synthetic trace with $Q=100$.

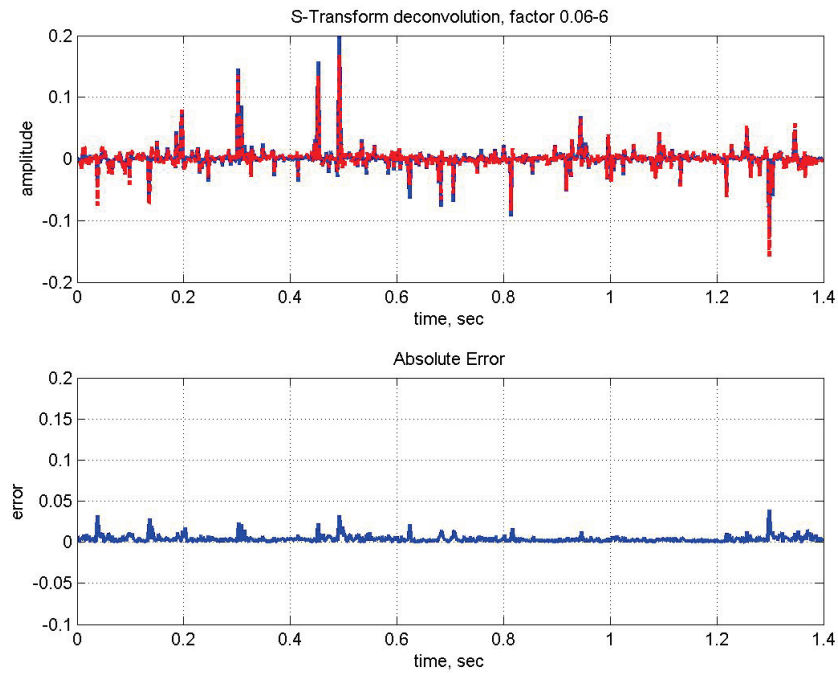


Figure 10: Variable factor S-transform deconvolution of the synthetic trace with $Q=100$.

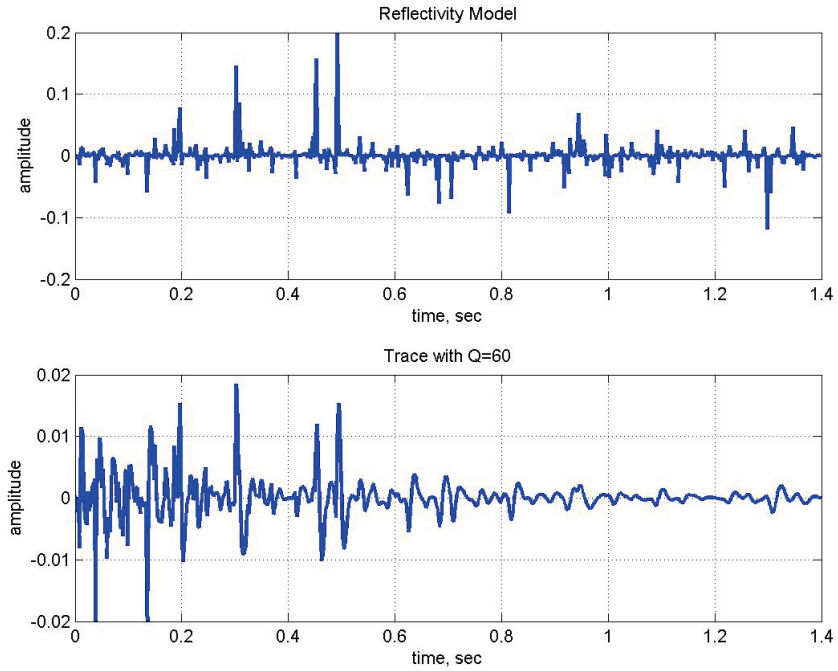


Figure 11: A random reflectivity model and a synthetic trace with a minimum-phase wavelet and $Q=60$.

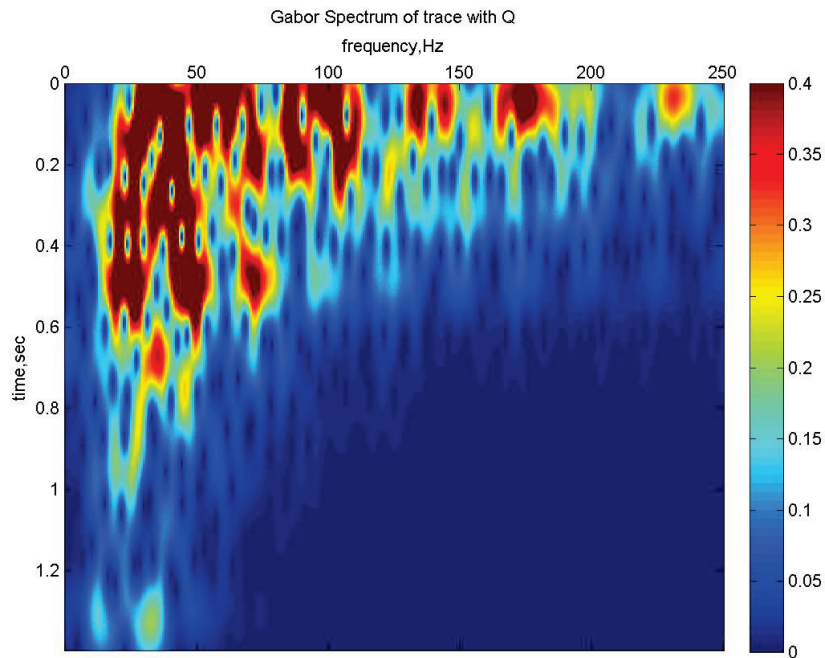


Figure 12: Gabor transform of the synthetic trace with $Q=60$.

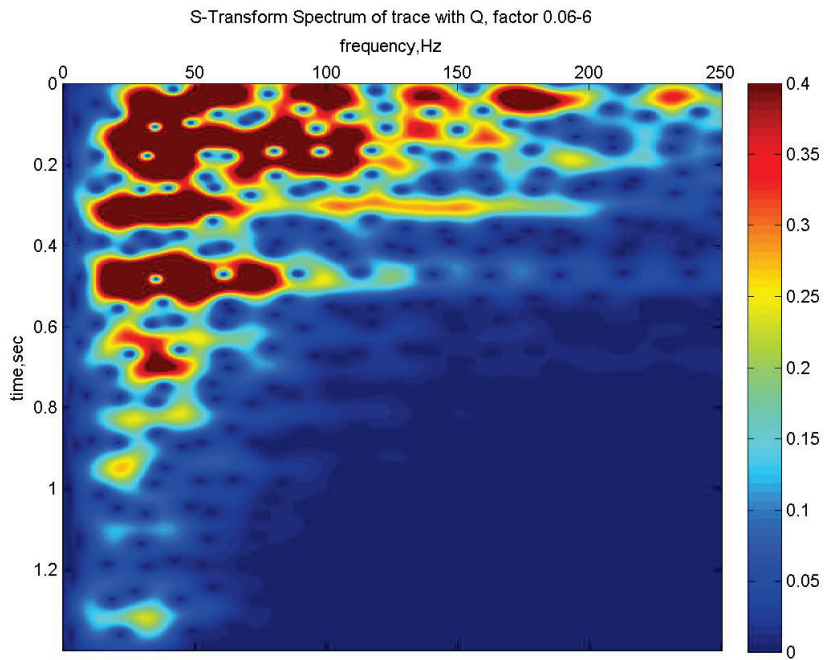


Figure 13: Variable factor S-transform of the synthetic trace with Q=60.

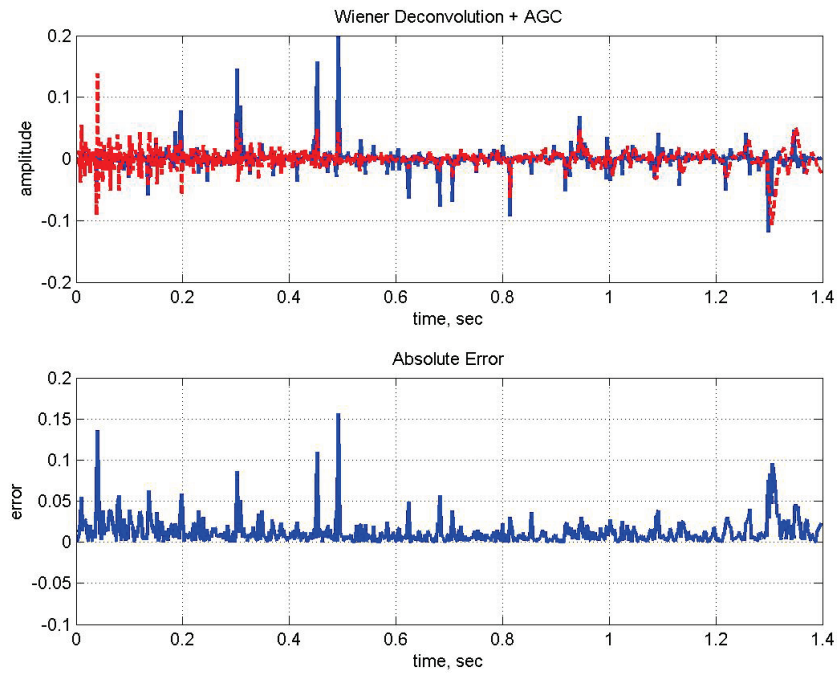


Figure 14: Wiener deconvolution of the synthetic trace with Q=60.

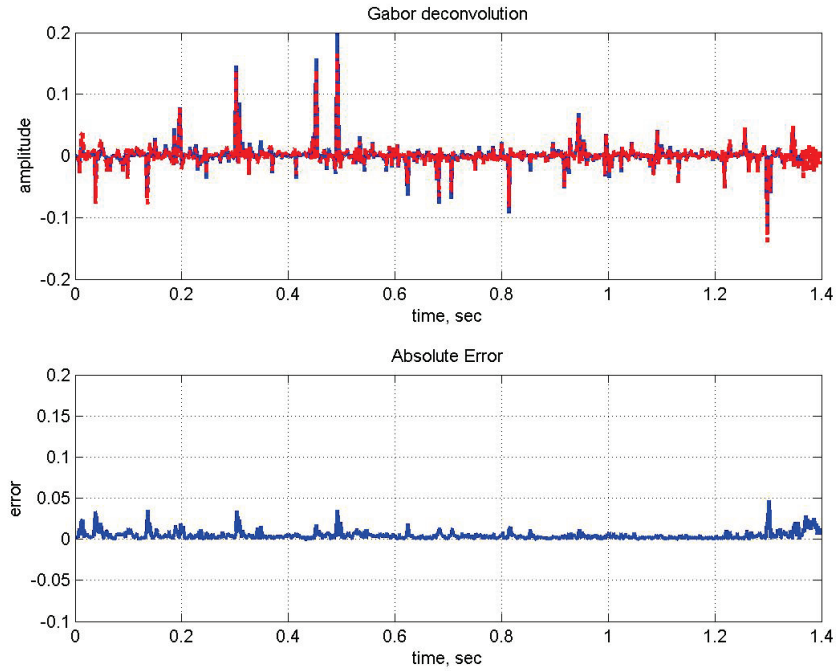


Figure 15: Gabor deconvolution of the synthetic trace with Q=60.

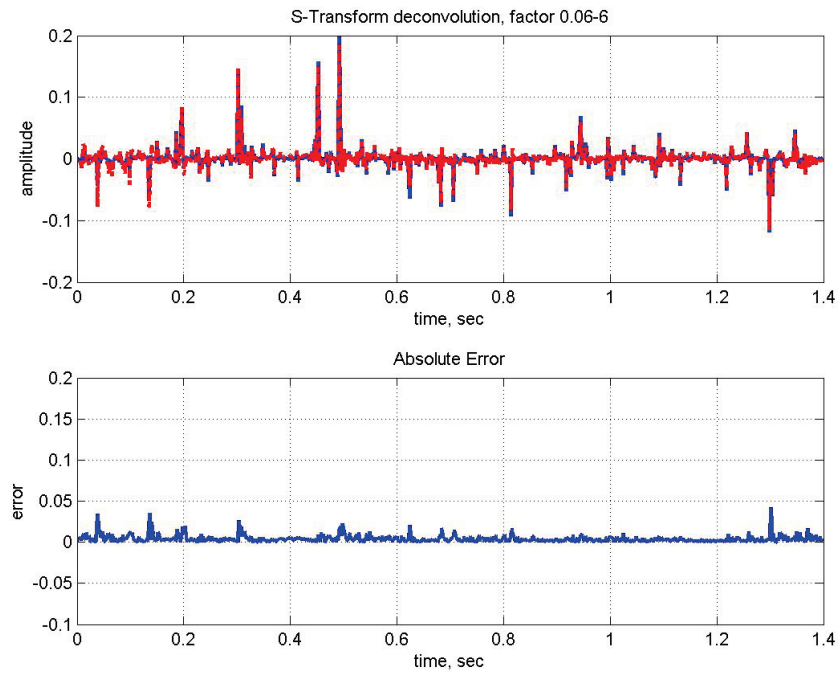


Figure 16: Variable factor S-transform deconvolution of the synthetic trace with Q=60.

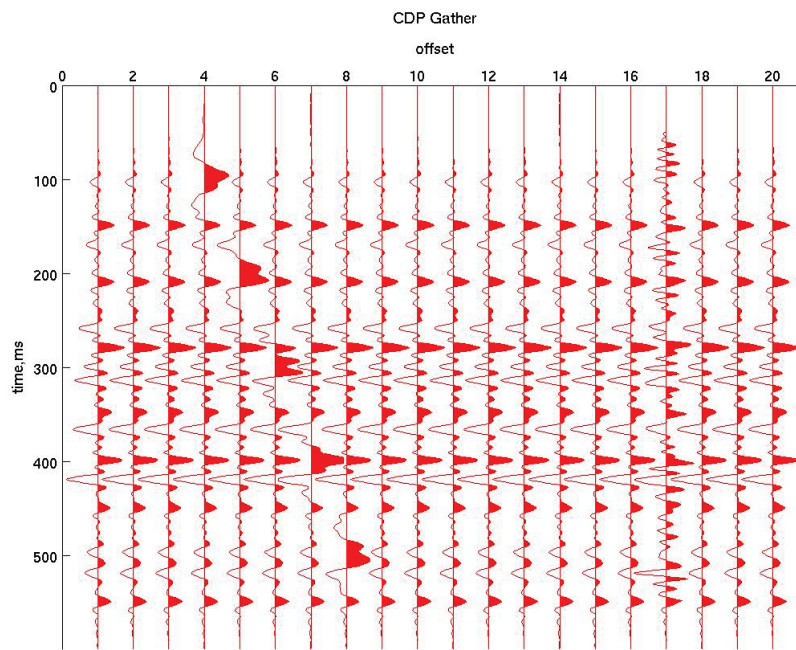


Figure 17: A synthetic CDP model with noise.

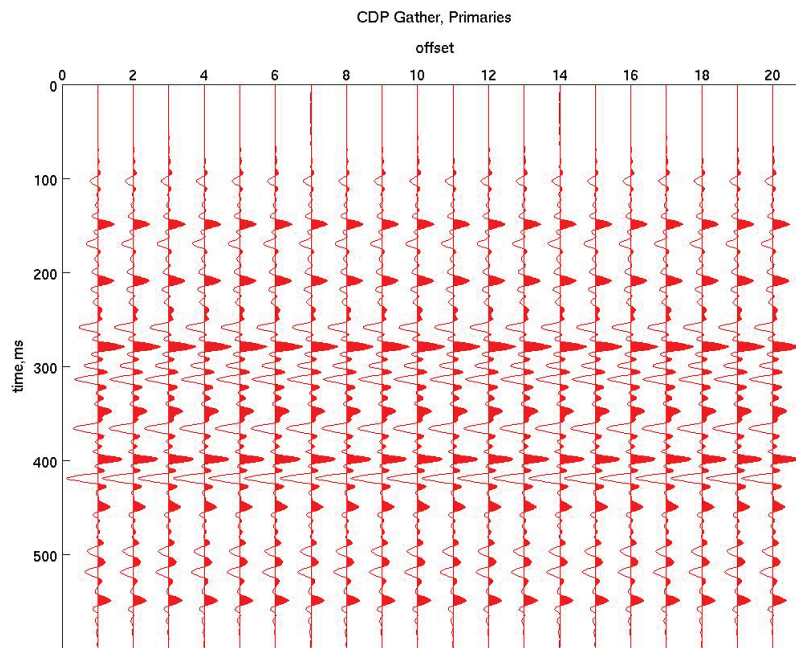


Figure 18: Primaries only of the CDP synthetic model.

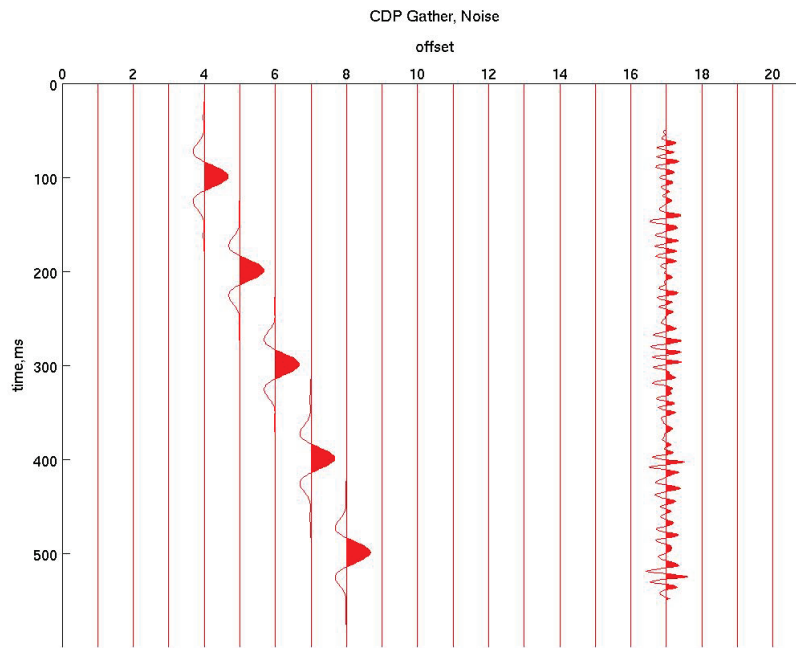


Figure 19: Noise only of the synthetic CDP model.

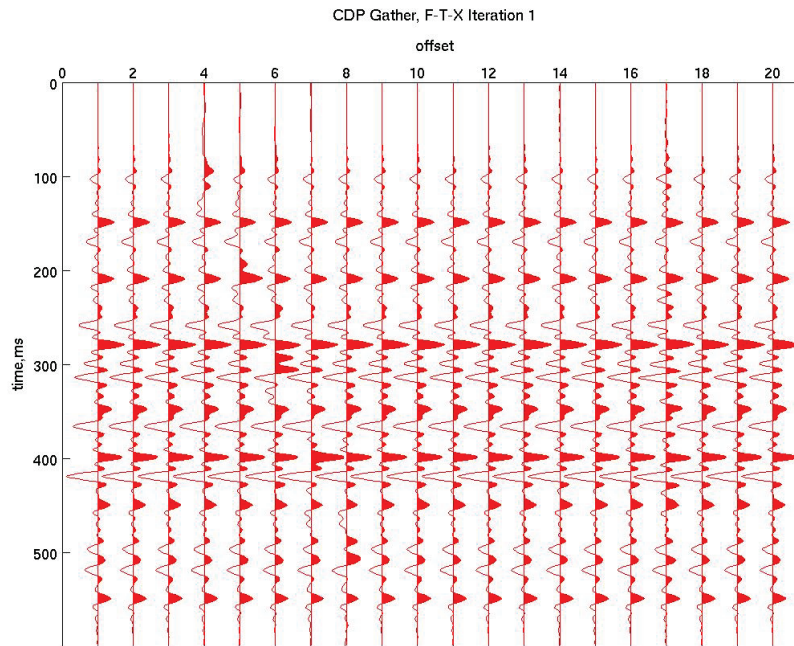


Figure 20: CDP model after a single iteration of the f-t-x noise attenuation.

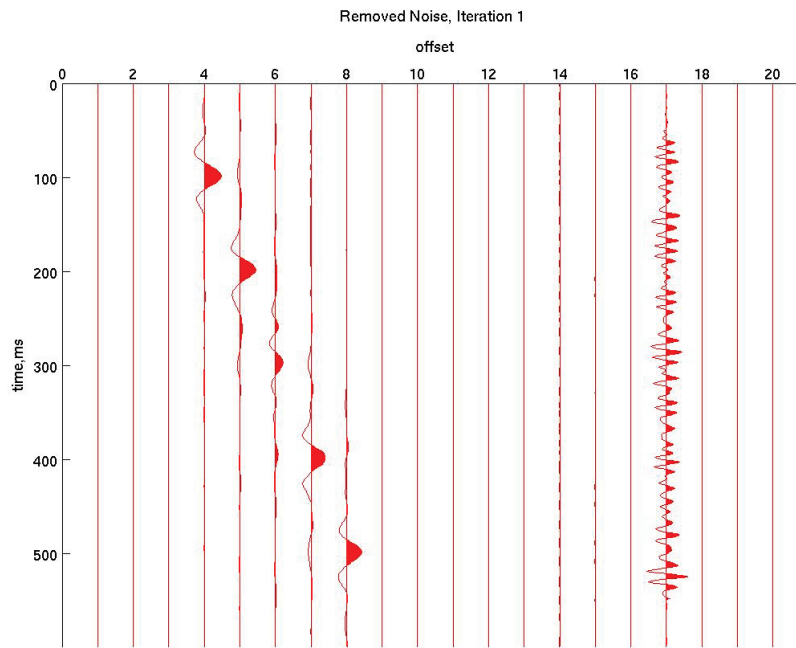


Figure 21: Noise removed after a single iteration.

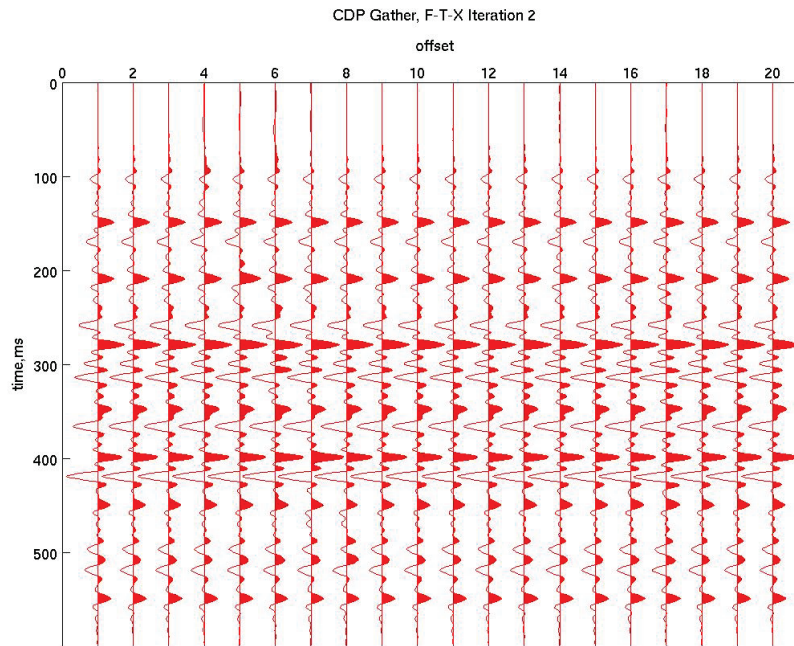


Figure 22: CDP model after a second iteration of the f-t-x noise attenuation.

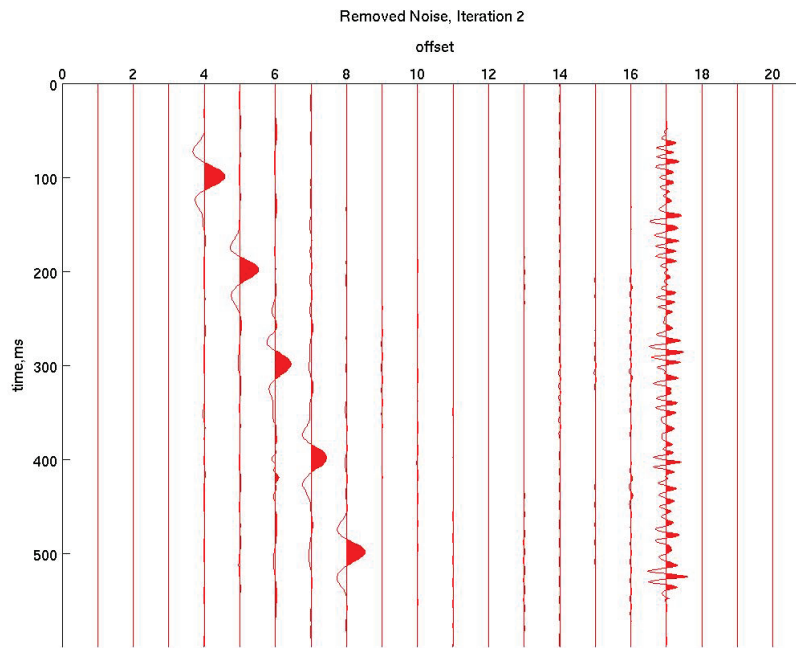


Figure 23: Noise removed after a second iteration.